BULLETIN OF THE POLISH ACADEMY OF SCIENCES
TECHNICAL SCIENCES, Vol. 67, No. 4, 2019
DOI: 10.24425/bpasts.2019.130191

The effect of material gradient on the static and dynamic response of layered functionally graded material plate using finite element method

N. VASIRAJA* and P. NAGARAJ

Department of Mechanical Engineering, Mepco Schlenk Engineering College, Sivakasi, India

Abstract. This article focuses on the finite element analysis (FEA) of the nonlinear behavior of a layered functionally graded material (FGM) plate as concerns displacement, stresses, critical buckling load and fundamental frequency. The material properties of each layer in an FGM plate are assessed according to a ceramic based simple power law distribution and the rules of mixture. The finite element model of a layered FGM plate is developed using ANSYS®15.0 software. The developed finite element model is used to study the static and dynamic responses of an FGM plate. In this paper, the effects of power law distribution, thickness ratio, aspect ratio and boundary conditions are investigated for central displacement, transverse shear stress, transverse normal stress, critical buckling load and fundamental frequency, and the obtained FEA results are in sound agreement with the literature test data results. Since the FGM is used in a high temperature environment, the FE analysis is performed for the FGM plate under a thermal field and then correlated. Finally, the FGM plate is analyzed under a thermomechanical load by using the current FE concept.

Key words: FGM plate, finite element, power law index, buckling load, fundamental frequency, ANSYS®.

1. Introduction

In recent decades, there has appeared a wide range in FGMs plates which are a heterogeneous composite made of two constituents, i.e. ceramic and metal one, with both the composition and material properties varying gradually through the thickness of the plate. The finite element method (FEM) is used for the calculation of the central deflection, plane stresses, transverse shear stress, critical buckling load and natural frequencies of FGM plates with different volume fractions of two constituent materials and it requires large computational efforts.

Reddy [1] has used third order shear deformation plate theory to analyze the static response of FGM rectangular plates. Qian et al. [2] have employed the higher order shear and normal deformable plate theory along with the Meshless Local Petrov-Galerkin method (MLPG) to analyze thick FGM plates. The static behavior of FGM plates using a generalized shear deformation theory has been investigated by Zenkour [3]. An interesting review of the modeling and analysis of FGMs has been prepared by Birman et al. [4]. Matsunaga [5] examined the bending behavior of thick FGM plates using the shear deformable theory with higher order. Talha et al. [6] developed higher order shear deformation theory based on an isoparametric element with a nine node to investigate the bending and vibration response of FGM plate. Singha et al. [7] investigated the nonlinear bending analysis of FGM plates under transverse distributed load. The authors assumed grading in the thickness direction using simple power law distribution with respect to the power law index. Rao et al. [8] have performed the finite element modeling and analysis of an FGM shell structure under different mechanical, thermal and free vibration conditions. Thai et al. [9] have developed a four-node quadrilateral finite element using Lagrangian and Hermitian interpolation functions, and presented different shear deformation theory for the bending and vibration analysis of FGM plates. Daouadji et al. [10] developed new higher shear deformation theory using the Navier solution to investigate the static behavior of an FGM plate for various boundary conditions, the aspect ratio and thickness ratio. Yang et al. [11] have investigated vibration and buckling of FGM plates subjected to an initial stress by higher order shear deformation theory. Zhao et al. [12] have presented the mechanical and thermal buckling analysis of functionally graded ceramic-metal plates which contain a square and circular hole for finding the influence of the size of the hole on buckling strength. Latifi et al. [13] have investigated the buckling of thin rectangular FGM plates using the double Fourier series procedure and Stokes' transformation. Rad et al. [14] have obtained a critical buckling load of functionally graded plates containing a crack using classical plate theory by FEM, and have shown numerically that the critical load decreases as the power law index increases.

Abrate [15] obtained natural frequencies, buckling loads and static deflections of FG plates from the corresponding results for isotropic plates without direct analysis of FG plates. Matsunaga [16] carried out an analysis of the stability and free vibration of FGM plates using two-dimensional higher order deformation theory. Zhao et al. [17] have presented a method for analyzing the free vibration of an FGM plate using the element-free kp-Ritz method for various boundary conditions, which has already been successfully implemented in the analysis of isotropic and composite plates. Efraim [18] derived an

*e-mail: vasiraja@mepcoeng.ac.in

Manuscript submitted 2018-07-28, revised 2018-10-03 and 2018-10-10, initially accepted for publication 2018-10-16, published in August 2019

empiric accurate formula that gives a correlation between the fundamental frequencies of an FGM plate and isotropic plate, even with different Poisson's ratio and with less computational efforts. Javaheri et al. [19] studied the buckling behavior of simply supported rectangular FGM plates. Chu et al. [20] investigated buckling analysis of thin FGM plates based on the collocation method associated with radial basis function. The application and characterization of FGM plates have been indicated by Malik et al. [21] and Chmielewski et al. [22]. Zur [23] has performed frequency analysis of a thin circular plate using the Green's function approach. Timoshenko et al. [24] explained the fundamental theory of plates and shells. Zhang et al. [25] applied theoretical analysis to a thin functionally graded material plate based on the physical neutral surface. Taj et al. [26] used higher deformation theory to analyze static behavior of FGM under an FGM plate and skew plate. Zhang [27] has successfully modelled an FGM rectangular plate using higher shear deformation theory. Lal et al. [28] explained vibration analysis of an axisymmetric FGM model. Parandvar et al. [29] proposed and analyzed dynamic response of an FGM plate under static, thermal and harmonic load. Zur used quasi-Green's function to analyze an elastically supported FGM circular plate [30] and annular plate [31].

In recent literature, the mathematical modeling of a basic 2D structure of FGM has been established very well while for the 3D part the FGM profile is very limited. In the case of a complex engineering structure, i.e. a gas turbine blade or aircraft fuselage, it is mandatory to carry out finite element analysis of the 2D and 3D structure of FGM. Since to date very limited literature is available on 2D and 3D mathematical modelling of FGM under a thermal field, an attempt has been made to develop an FE model, based on the commercial FEA ANSYS®15.0 package. With this in mind, the principal goal of the present paper has been established as to develop a finite element model using ANSYS®15.0 and demonstrate the accuracy of the current FE model with analytical and numerical results. Initially the obtained results for bending, buckling and free vibration behavior of FGM plates with a varying power law index, boundary conditions, aspect ratio and thickness ratio have been correlated. Since the premier application of FGM is under a thermal field, FE analysis on central deflection of an FGM plate under a thermal field has also been done and validated. In view of producing new results, the FE analysis of an FGM plate has been performed under thermo-mechanical load using the current FE model.

2. Evaluation of effective material properties of FGM plate along thickness direction

The FGM plate which is modeled as a mixture of ceramic material and metal with thickness 'h' is shown in Fig. 1. The material on the bottom surface ($z = -h/2$) of the plate is rich in ceramic components whereas the top surface ($z = h/2$) material is rich in metal. Here 'z' is the distance measured from the middle of the plate. In the current FGM plate model, the effective properties of the modulus of elasticity, mass density and the

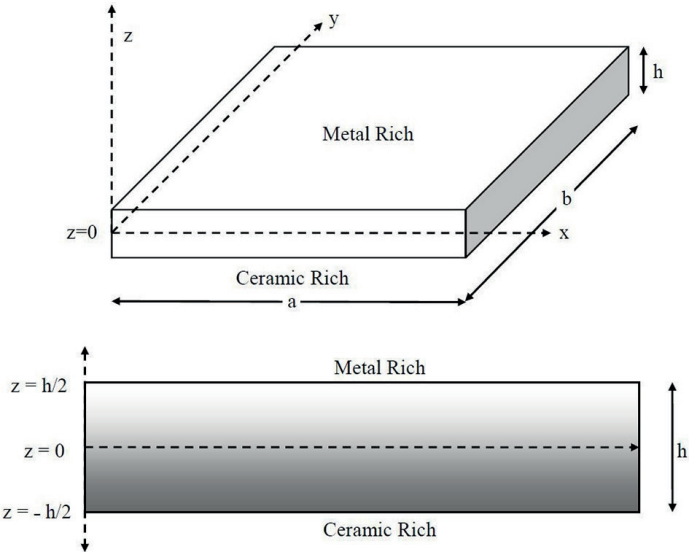

Fig. 1. Schematic representation of FGM plate

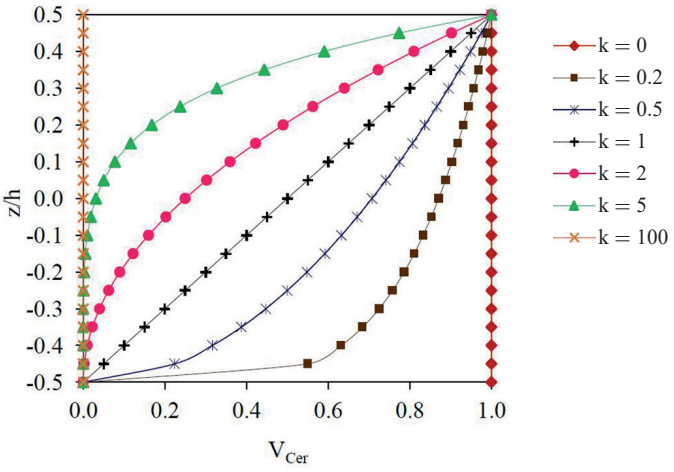

Fig. 2. Variation of volume fraction of ceramic material through thickness

Poisson's ratio for each layer are evaluated by the simple rule of mixtures techniques as represented in Equation 1 to Equation 3. The volume fractions of constituents of ceramic (V_{Cer}) is calculated using Equation 4 and shown in Fig. 2.

$$E(z) = E_{Cer}V_{Cer} + E_{Met}V_{Met} \tag{1}$$

$$v(z) = v_{Cer}V_{Cer} + v_{Met}V_{Met} \tag{2}$$

$$\rho(z) = \rho_{Cer}V_{Cer} + \rho_{Met}V_{Met} \tag{3}$$

$$V_{Cer} = \left[\frac{1}{2} + \frac{z}{h}\right]^{k}. \tag{4}$$

In Equation 4 the power law index parameter, 'k', commands material distribution through the thickness of the plate that takes on values greater than or equal to zero. Accordingly,

the bottom surface ($z = -h/2$) of the plate is modeled as purely ceramic while the top surface ($z = h/2$) is modeled as pure metal and for different value of k, thus different volume fraction of the ceramic material would be obtained. It can also be noted that the plate becomes isotropic, and the material properties of all layers are the same while setting $k = 0$ or ∞. The V_{Met} is determined based on a simple rule of mixture shown in Equation 5.

$$V_{Cer} + V_{Met} = 1. \tag{5}$$

3. Finite element modeling of FGM plate

In the present paper, the finite element formulation for the FGM plate has been completed using ANSYS®15.0 software. The Shell181 element is a layered element used to model the FGM plate with a layer concept. It is the four node element with each node having six degrees of freedom (translation and rotation about the x, y and z axes). This element is governed by first order shear deformation theory (Mindlin-Reissner shell theory). It accepts surface load (pressure) and body load (temperature) and also stores variables of all layers. It is able to produce nodal displacement, shear force, bending moment, in-plane stresses, shear stresses and also interlaminar shear stresses. Details of the FE analysis (analysis type, element type, materials, boundary and loading conditions) are presented in Table 1. In this model, a finite portion of the thickness is considered as each layer and treated as an isotropic material. Material properties have been evaluated in the middle of each layer by using power law index grading. A twenty-layer shell element has been used for the FGM plate. A typical FE model of the FGM plate with the boundary conditions is shown in Fig. 3. In Figure 4, the different colors indicate the number of layers with different material properties.

3.1. Convergence study. Initially, the convergence study for the current FE model is done for nondimensional central displacement $(\bar{W}_c)$, maximum bending moment $(\bar{M}_x)$, maximum shear force $(\bar{Q}_{xz})$ and maximum transverse shear stress $(\bar{\tau}_{xz\,max})$ of a simply supported thin (when $a/h = 100$) isotropic square

Table 1
Finite element model and analysis description

Parameter	Description
Software package used	ANSYS® 15.0
Analysis type	structural- static, modal, buckling and thermo-mechanical (coupled field)
Element name	Shell181 (structural analysis) Shell131 (thermal analysis)
Material used	Static analysis : Aluminum (Al) and Alumina (Al_2O_3) Thermo-mechanical: Aluminum (Al) and Zirconia (ZrO_2)
Material properties	Given in Table 2
Number of layers	20
Layer material properties	Varying from bottom to top by simple exponential power law index (k) and each layer is considered isotropic
Loading condition	Transverse uniformly distributed load (q_0) and thermal field (bottom surface temperature = 20°C and top surface temperature varying from 20°C to 300°C
Boundary condition	SSSS (simply supported) at $x = 0$ and a: $v = w = \varphi y = 0$ at $y = 0$ and b: $u = w = \varphi x = 0$ CCCC (clamped) at $x = 0$ and a: $u = v = w = \varphi x = \varphi y = \varphi z = 0$ at $y = 0$ and b: $u = v = w = \varphi x = \varphi y = \varphi z = 0$

Table 2
Material Properties

Material	E (GN/m^2)	ν	ρ (kg/m^3)	K (W/m K)	α (m/K)
Aluminum	70	0.3	2707	204	23×10^{-6}
Alumina	380	0.3	3800	10.4	7.4×10^{-6}
Zirconia	151	0.3	3000	2.09	10×10^{-6}

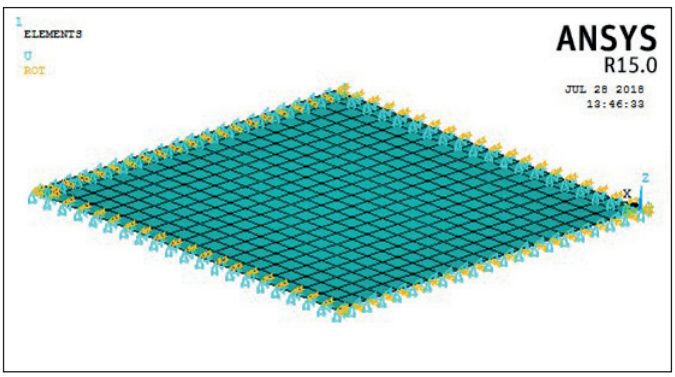

Fig. 3. FE model of FGM plate using ANSYS® shell 181 element

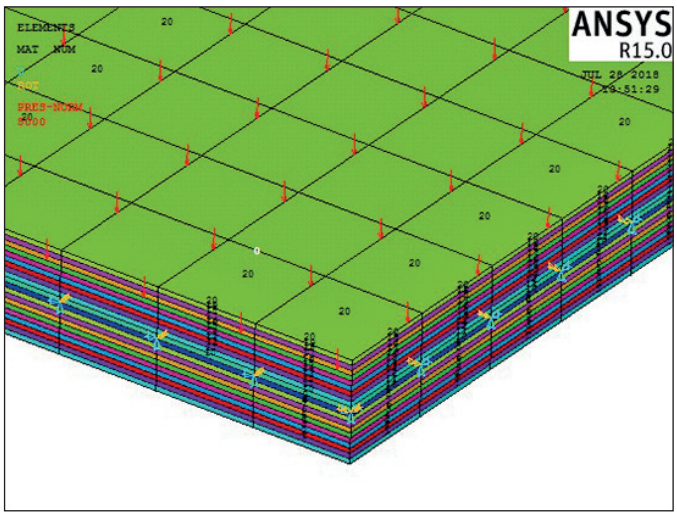

Fig. 4. FE model of FGM plate with 20 layers

plate under transverse uniformly distributed load (UDL) q_0 and compared with the analytical solution presented by Timoshenko et al. [24]. The following equations are used to evaluate the nondimensional parameter unless indicated otherwise. It is found from this that reasonable convergence is attained with 50×50 numbers of finite elements, as shown in Table 3.

Table 3
Convergence study of FE model

Non-dimensional parameter	Current analysis results for various mesh sizes					Timoshenko [24]
	10×10	20×20	30×30	40×40	50×50	
$\bar{W}_c$	0.00406	0.00406	0.00406	0.00406	0.00406	0.00406
$\bar{M}_x$	0.04680	0.04779	0.04785	0.04787	0.04788	0.04790
$\bar{Q}_{xz}$	0.28920	0.32117	0.32772	0.33055	0.33350	0.33730
$\bar{\tau}_{xz\,max}$	0.43385	0.48176	0.49158	0.49582	0.50025	0.50200

4. Simulation results and discussion

4.1. Bending analysis of isotropic plate and validation. Initially, the current FE model was validated for center deflections, in-plane stress and shear stress of isotropic plates with different thickness ratios (a/h = 10 and 100). Table 4 indicates that center deflections matched well for thin and thick plates and Table 5 shows the ability of the current FE model to evaluate in-plane stress and shear stress of plate along thickness direction. Based on the results that are closer to the literature test data, it is revealed that the current FE model could be used for analyzing the thin (a/h = 10) and thick plate (a/h = 100).

Table 4
Center deflections of isotropic plates ($E_{Met} = E_{Cer} = 1$, $q_0 = 1$, and a/b = 1)

a/h	Present	Reddy [1]
100	44346.20	44383.87
10	46.62	46.65

Table 5
In-plane stress (σ_{xx}) and shear stress (τ_{xy}) of isotropic plate along thickness direction

a/h	z	σ_{xx}		τ_{xy}	
		Present	Reddy [1]	Present	Reddy [1]
100	0.005	2872.9	2873.4	1939.0	1949.0
	0.004	2298.3	2298.5	1551.2	1558.8
	0.003	1723.7	1723.8	1163.4	1168.8
	0.002	1149.1	1149.2	775.60	779.15
	0.001	574.57	574.59	387.80	389.54
	0.000	0.0000	0.0000	0.0000	0.0000
4	0.005	28.72	28.92	19.39	20.00
	0.004	22.98	23.00	15.51	15.62
	0.003	17.23	17.17	11.63	11.50
	0.002	11.49	11.41	7.758	7.565
	0.001	5.745	5.693	3.879	3.751
	0.000	0.000	0.000	0.000	0.000

4.2. Bending behavior of FGM plate. In this section, first the efficiency of the current FE model is assessed within static analysis of the FGM plate. Here the FGM plate is composed with aluminum as the metal and alumina as the ceramic component while the material properties of each layer are evaluated using Equation 1, 2 and 3 and fed into the FE model. FEA results corresponding to nondimensional central displacements, maximum shear stress and in-plane stress along x direction for the FGM plates with simply supported edges (SSSS) and clamped edges (CCCC) under transverse UDL are tabulated in Table 6a and 6b, and it is seen that the developed FEA results are discreetly matched with Singha et al. [7].

It is also observed that nondimensional central displacement increases with the increase in power law index, $k > 0$. This is due to the fact that the larger 'k' value means the plate has a smaller ceramic component and hence its stiffness is reduced. In addition to that, shear stress value increases with increasing of 'k' up to 1 and then decreases with further increasing of 'k' as shown in Table 6b.

Table 6a
Nondimensional central displacement $\bar{W}_c$ of SSSS and CCCC thin square FGM plate under q_0

Power law index	SSSS		CCCC	
	Present	Singha et al. [7]	Present	Singha et al. [7]
Ceramic	0.004064	0.004064	0.001237	0.001267
0.5	0.006236	0.006269	0.001949	0.001955
1	0.008136	0.008154	0.002540	0.002542
2	0.010447	0.010449	0.003264	0.003258
5	0.012388	0.012359	0.003870	0.003854
Metal	0.022048	0.022064	0.006883	0.006881

Table 6b
Nondimensional maximum shear stress and in-plane stress of SSSS and CCCC thin square FGM plate under q_0

Power law index	SSSS		CCCC	
	$\bar{\tau}_{xz\,max}$	$\bar{\sigma}_{xx}$	$\bar{\tau}_{xz\,max}$	$\bar{\sigma}_{xx}$
Ceramic	0.502760	28.728	0.638044	28.308
0.5	0.526720	37.196	0.665576	36.652
1	0.542260	43.456	0.692580	42.822
2	0.539220	49.884	0.665902	49.154
5	0.504100	55.214	0.603208	54.402
Metal	0.502760	28.728	0.638044	28.308

Figure 5 and 6 represent the variation of nondimensional central deflection with power law index for the FGM square plates having SSSS and CCCC boundary conditions, respectively. The lower k value has low deflection due to high stiffness while the higher k value has high deflection due to low stiffness. The variation of nondimensional in-plane stress through the thickness of a thin square FGM plate under UDL is analyzed and the results are shown in Fig. 7 for various values of the power law index. It is noticed that the through-thickness variation of in-plane stress is linear for the isotropic plate

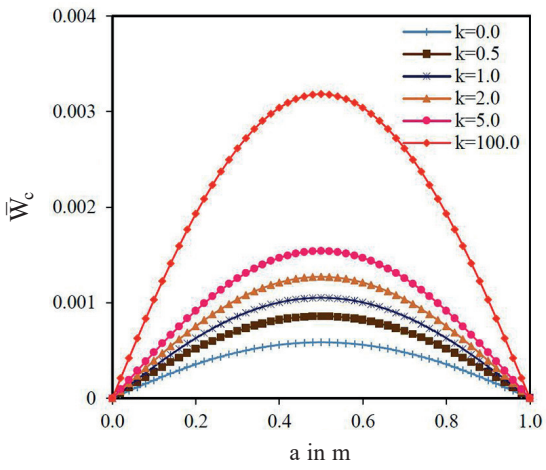

Fig. 5. $\bar{W}_c$ for SSSS thin FGM square plates under q_0

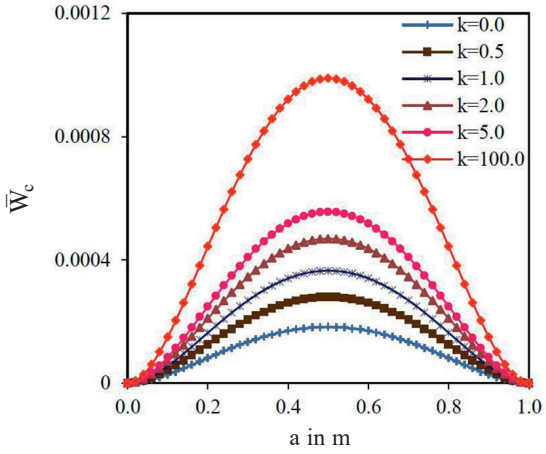

Fig. 6. $\bar{W}_c$ for CCCC thin FGM square plates under q_0

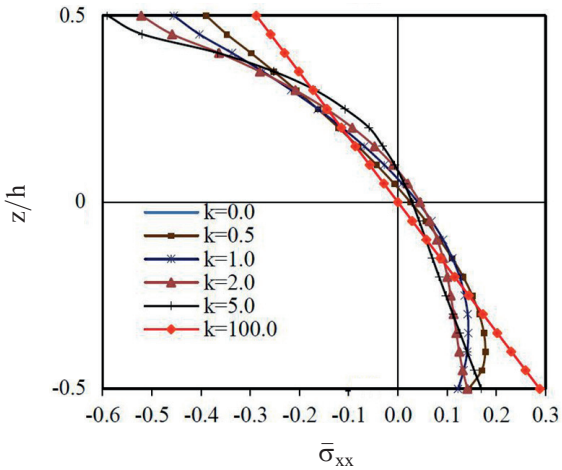

Fig. 7. Variation of $\bar{\sigma}_{xx}/100$ through thickness for SSSS thin FGM square plates under q_0

(k = 0 and 100) and becomes non-linear for the in-between value of k. The effect of power law index on transverse shear stress through the thickness variation is highlighted in Fig. 8. It is observed that the variation of transverse shear stress ($\bar{\tau}_{xz}$)

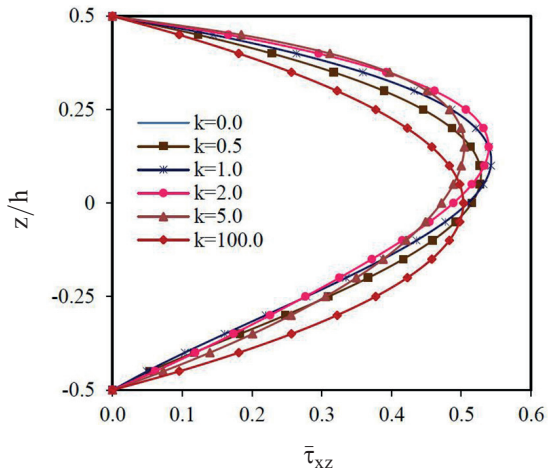

Fig. 8. Variation of $\bar{\tau}_{xz}$ through thickness for SSSS thin FGM square plates under q_0

through the thickness is parabolic in general and maximum in the middle of the thickness for the isotropic plate (k = 0 and 100). But for the remaining 'k' value, the peak of transverse shear stress does not occur in the middle due to unsymmetrical material properties along the thickness direction.

The capability of the current FE formulation is also tested for the SSSS thick FGM plate (Al/Al_2O_3) subjected to q_0. The nondimensional central displacement, in-plane stress and shear stress values evaluated here were compared with those of the generalized shear deformation theory in Table 7a, and it has been found that the results matched very well. Then the in-plane stress and shear stress results were also obtained for the CCCC boundary condition, as presented in Table 7b.

Table 7a
Nondimensional central displacement $\bar{W}_c$, in-plane stress $\bar{\sigma}_{xx}$ and shear stress $\bar{\tau}_{xz}$ of SSSS thick FGM square plate under q_0

Power law index	$\bar{W}_c$		$\bar{\sigma}_{xx}$		$\bar{\tau}_{xz}$	
	Present	Zenkour [3]	Present	Zenkour [3]	Present	Tahar et al. [10]
Ceramic	0.466	0.466	2.872	2.868	0.491	0.5072
0.5	0.712	—	3.719	—	0.501	—
1	0.927	0.929	4.345	4.430	0.491	0.5072
2	1.193	1.195	4.988	5.168	0.466	0.4651
5	1.444	1.435	5.521	5.891	0.427	0.4128
Metal	2.530	2.530	2.872	2.868	0.491	0.5072

Table 7b
Nondimensional central displacement $\bar{W}_c$, in-plane stress $\bar{\sigma}_{xx}$ and shear stress $\bar{\tau}_{xz}$ for CCCC thick FGM square plate under q_0

Power law index	$\bar{W}_c$	$\bar{\sigma}_{xx}$	$\bar{\tau}_{xz}$
Ceramic	0.16416	2.73574	0.60242
0.5	0.24776	3.55542	0.63158
1	0.32148	4.15828	0.63278
2	0.41800	4.76128	0.60416
5	0.52136	5.21704	0.56374
Metal	0.88920	2.73574	0.60242

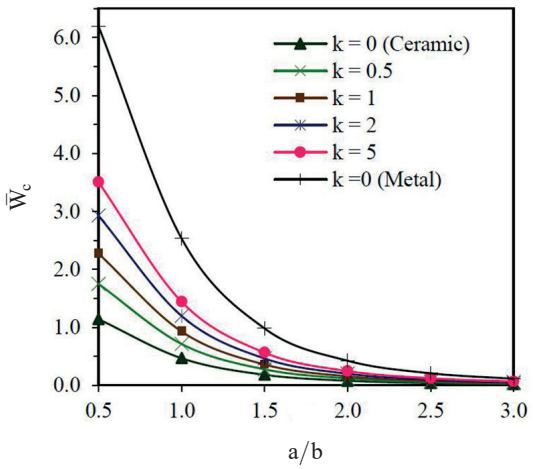

Fig. 9. Variation of $\bar{W}_c$ as function of aspect ratios for a/h = 10 under q_0

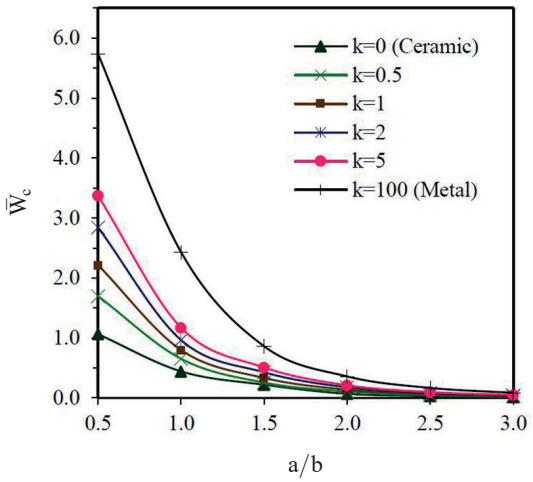

Fig. 10. Variation of $\bar{W}_c$ as function of aspect ratios for a/h = 100 under q_0

Table 8
Nondimensional central displacement $\bar{W}_c = 10W_cE_{Cer}h^3/q_0a^4$ of FGM plate for different aspect ratios

a/h	a/b	Power law index					
		k = 0	k = 0.5	k = 1	k = 2	k = 5	k = 100
10	0.5	1.140	1.748	2.272	2.926	3.503	6.194
	1.0	0.466	0.712	0.928	1.196	1.441	2.533
	1.5	0.180	0.275	0.358	0.462	0.562	0.980
	2.0	0.078	0.117	0.153	0.199	0.244	0.423
	2.5	0.038	0.057	0.074	0.096	0.120	0.206
	3.0	0.020	0.030	0.040	0.052	0.066	0.112
100	0.5	1.064	1.698	2.216	2.844	3.371	5.735
	1.0	0.443	0.653	0.799	0.966	1.171	2.432
	1.5	0.220	0.256	0.333	0.428	0.508	0.861
	2.0	0.069	0.106	0.138	0.177	0.2113	0.358
	2.5	0.032	0.049	0.063	0.082	0.098	0.167
	3.0	0.016	0.025	0.033	0.042	0.050	0.085

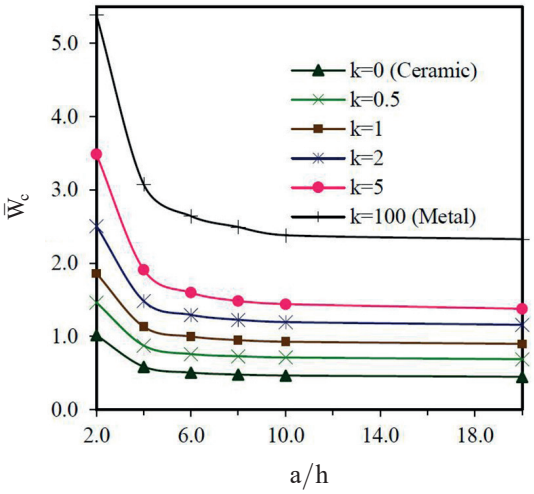

Fig. 11. Variation of $\bar{W}_c$ for different thickness ratios under q_0

The current FE model aims to investigate the effect of aspect ratio (a/b) on central displacement of the FGM plate. Table 8 and Fig. 9 and 10 show the variation of nondimensional center deflection of the FGM plate with different aspect ratios for a simply supported thin and thick FGM plate, respectively. Central displacement is at its maximum for the metallic plate (k = 100) and at its minimum for the ceramic plate (k = 0). The difference increases as the aspect ratio increases while it may remain unchanged with the increase of thickness ratio. One of the main inferences from the FE analysis is that the response of FGM plates is intermediate to that of the ceramic and metal homogeneous plates. Figure 11 exhibits central displacement for varying thickness ratios and implies that it may remain unchanged despite increasing the thickness ratio beyond a/h = 10.

Figure 12 shows that the distributions of in-plane stress through the thickness are compressive throughout the plate up to z = 0.150 and after that the stress become tensile. Figure 13 and 14 show the distributions of shear stresses $\bar{\tau}_{xz}$ and $\bar{\tau}_{xy}$ through the thickness. The power law index of the FGM plate is assumed as k = 2 in these figures. The distributions of shear stresses $\bar{\tau}_{xz}$

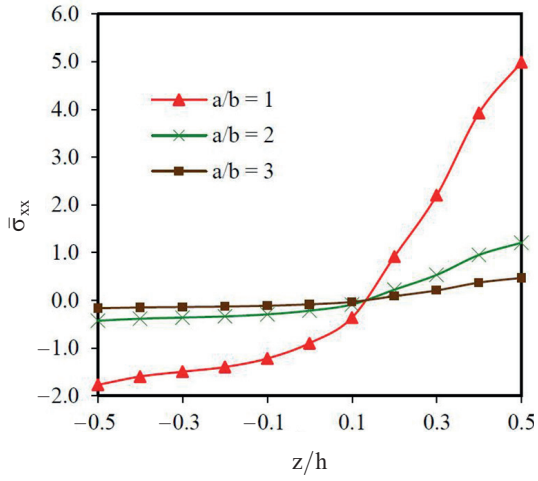

Fig. 12. Variation of $\bar{\sigma}_{xx}$ as for different aspect ratios under q_0

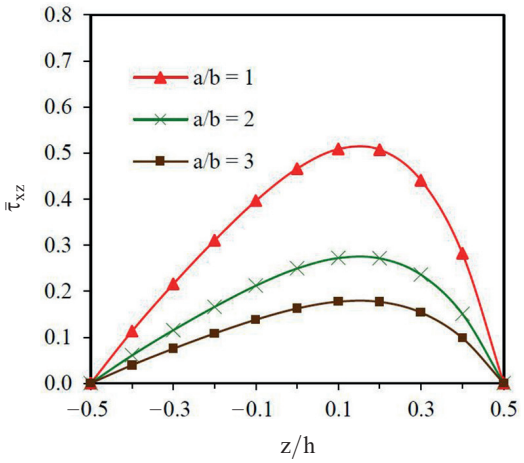

Fig. 13. Variation of $\bar{\tau}_{xz}$ for different aspect ratios under q_0

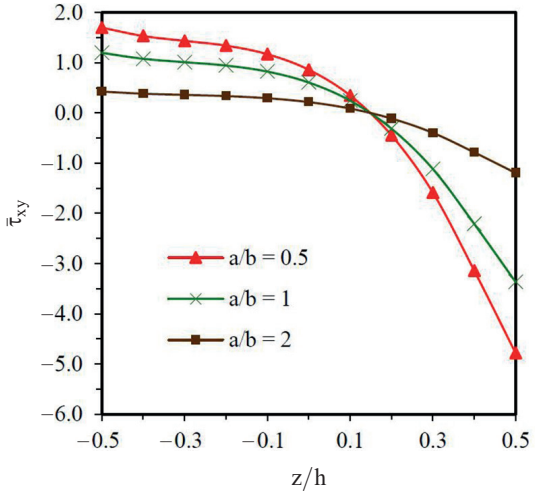

Fig. 14. Variation of $\bar{\tau}_{xy}$ for different aspect ratios under q_0

through the thickness are not parabolic and the stresses increase as the aspect ratio decreases. It also needs to be noted that the maximum value of shear stress occurs at z = 0.198, not in the middle of the plate as in the case of the isotropic plate.

4.3. Buckling behavior of FGM plate. Critical buckling loads of an FGM plate with SSSS edges under unidirectional compression for different power law index and aspect ratios are obtained by using the current FE model and the comparison of the results with those obtained by Javaheri et al. [19]. They are presented in Table 9. The results appear to match each other very closely. The plate become isotropic with the highest possible stiffness while 'k' equals zero, and increase in the FGM power law index causes the portion of metal to be more pronounced, leading to a decrease in plate stiffness. As a result, for each aspect ratio in Table 9, the greatest buckling load, corresponding to k = 0, decreases with the increase in the power law index. In addition, the buckling load increases with an increase in the aspect ratio for each FGM power index due to increasing the a/b ratio. The plate becomes shorter in the direction of the compressive load while the length a is constant. Additionally, critical buckling loads of the FGM plate with CCCC edges are evaluated and tabulated in Table 10. The results are higher than for the FGM plate SSSS edges due to stability of the clamped condition.

Table 9
Critical buckling loads $(\times 10^5\ \mathrm{N/m})$ of FGM plate with SSSS edges

a/b	Model	Power law index				
		k = 0	k = 0.5	k = 1	k = 5	k = 100
1	Present	6.820	4.444	3.407	2.234	1.257
	Javaheri et al. [19]	6.805	—	3.390	2.240	—
1.5	Present	7.982	5.201	3.987	2.614	1.471
	Javaheri et al. [19]	7.984	—	3.973	2.621	—
2	Present	10.643	6.934	5.316	3.485	1.961
	Javaheri et al. [19]	10.632	—	5.310	3.511	—
2.5	Present	14.322	9.332	7.154	4.690	2.638
	Javaheri et al. [19]	14.311	—	7.134	4.722	—
3	Present	18.934	12.337	9.458	6.201	3.488
	Javaheri et al. [19]	18.921	—	9.430	6.221	—

Table 10
Critical buckling loads $(\times 10^5\ \mathrm{N/m})$ of FGM plate with CCCC edges

a/b	Model	Power law index					
		k = 0	k = 0.5	k = 1	k = 2	k = 5	k = 100
1	Present	17.273	11.249	8.622	6.716	5.662	3.182
	Javaheri et al. [19]	17.261	—	8.608	6.715	5.671	—
1.5	Present	22.400	14.590	11.184	8.711	7.341	4.126
	Javaheri et al. [19]	22.432	—	11.180	8.721	7.380	—
2	Present	33.065	21.542	16.515	12.861	10.833	6.091
	Javaheri et al. [19]	33.040	—	16.473	12.852	10.871	—
2.5	Present	47.692	31.083	23.833	18.558	15.618	8.785
	Javaheri et al. [19]	47.660	—	23.761	18.542	15.681	—
3	Present	65.931	42.988	32.967	25.667	21.579	12.145
	Javaheri et al. [19]	65.840	—	33.610	26.222	22.171	—

Figure 15 shows the variation of critical buckling load for different aspect ratios for the simply supported FGM plate

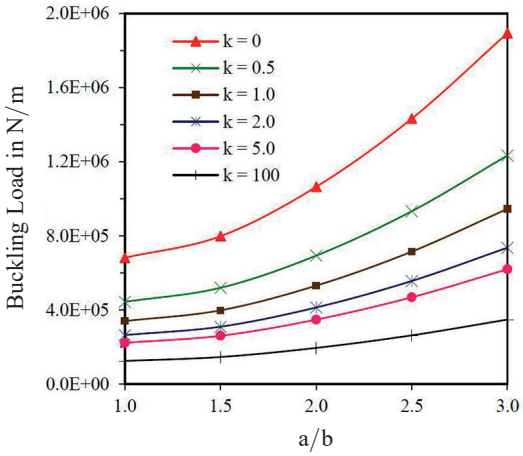

Fig. 15. Variation of critical buckling load for different aspect ratios of SSSS thick FGM plate

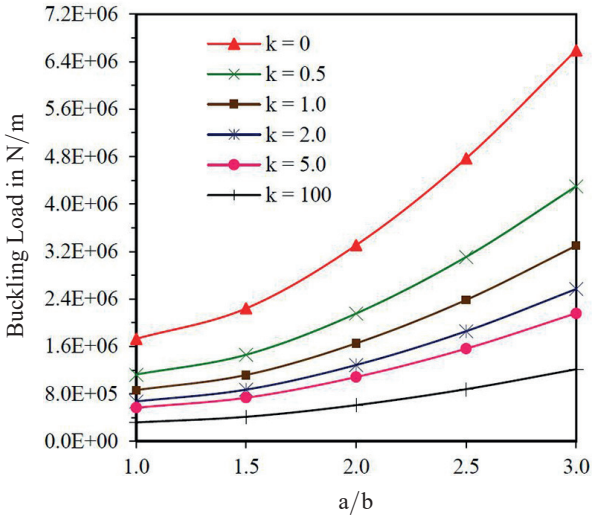

Fig. 16. Variation of critical buckling load for different aspect ratios of CCCC thick FGM plate

while Fig. 16 represents the clamped conditions. The difference in critical buckling load increases with the aspect ratio due to more of the power law index having minimum ceramic constituents.

4.4. Fundamental frequency of FGM plate. The natural frequencies of FGM plates with different material properties, aspect ratios and support conditions are examined in this section. The first ten natural frequencies for square plates with SSSS boundary conditions for k = 0, 0.5, 1, 2, 5 and ∞ are obtained, and the thickness of the plate is considered as 0.1

Table 11
Dimensionless frequency parameter (Ω) for SSSS FGM square plate

a/b	Method	Mode No.	Power law index				
			Ceramic	0.5	1	5	Metal
5	Matsunaga	1	0.21210	0.18190	0.16400	—	0.10770
	[16]	1	0.21113	0.18010	0.16645	0.13762	0.10736
	Present	2	0.38955	0.34038	0.32298	0.25103	0.19809
		3	0.38955	0.34038	0.32298	0.25103	0.19809
		4	0.46178	0.40266	0.37274	0.29733	0.23482
		5	0.46178	0.40266	0.37274	0.29733	0.23482
		6	0.55088	0.48080	0.45547	0.35301	0.28013
		7	0.66750	0.58812	0.54522	0.42536	0.33943
		8	0.77954	0.67893	0.64125	0.49468	0.39641
		9	0.77954	0.67893	0.64125	0.49468	0.39641
		10	0.78889	0.69790	0.64759	0.49979	0.40118
10	Matsunaga	1	0.05777	0.04917	0.04427	—	0.02933
	[16]	1	0.05767	0.04816	0.04448	0.03782	0.02933
	Present	2	0.13764	0.11633	0.10748	0.09000	0.06999
		3	0.13764	0.11633	0.10748	0.09000	0.06999
		4	0.19476	0.17033	0.16184	0.12610	0.09904
		5	0.19476	0.17033	0.16184	0.12610	0.09904
		6	0.21120	0.18017	0.16651	0.13767	0.10740
		7	0.25753	0.22080	0.20413	0.16751	0.13096
		8	0.25753	0.22080	0.20413	0.16751	0.13096
		9	0.27543	0.24081	0.22871	0.17804	0.14006
		10	0.32298	0.27868	0.25773	0.20942	0.16424

Table 12
Dimensionless frequency parameter (Ω) for CCCC FGM square plate

a/b	Mode No.	Power law index				
		Ceramic	0.5	1	5	Metal
5	1	0.32098	0.27601	0.25643	0.20213	0.16322
	2	0.56041	0.49046	0.45610	0.34927	0.28497
	3	0.56041	0.49046	0.45610	0.34927	0.28497
	4	0.74613	0.65061	0.61543	0.46769	0.37941
	5	0.74613	0.65061	0.61543	0.47555	0.37941
	6	0.75247	0.66373	0.61768	0.47555	0.38264
	7	0.85779	0.76114	0.70832	0.53206	0.43621
	8	0.86965	0.76899	0.71630	0.53800	0.44224
	9	0.89233	0.77633	0.73200	0.56301	0.45377
	10	1.01761	0.90426	0.84227	0.62926	0.51747
10	1	0.09840	0.08274	0.07656	0.06362	0.05004
	2	0.18779	0.15983	0.14803	0.12061	0.09549
	3	0.18779	0.15983	0.14803	0.12061	0.09549
	4	0.26318	0.22584	0.20928	0.16849	0.13383
	5	0.31030	0.26759	0.24807	0.19793	0.15779
	6	0.31327	0.26986	0.25020	0.19982	0.15930
	7	0.37271	0.32476	0.30140	0.23855	0.18953
	8	0.37271	0.32476	0.30140	0.23855	0.18953
	9	0.37517	0.32607	0.30923	0.24076	0.19078
	10	0.37517	0.32607	0.30923	0.24076	0.19078

m. The two thickness ratios a/h = 5 and 10 and two types of boundary conditions, i.e. SSSS and CCCC, have been selected.

Table 11 shows the variation of the dimensionless frequency parameter $\Omega = \omega h \sqrt{\rho_{Cer}/E_{Cer}}$ with the power law index for the FGM plates. The results for the first ten modes are computed. In the case of the plate with the SSSS boundary condition, the frequencies in all ten modes decrease as the power law index k increases, with the trend becoming gentler as 'k' increases, which is anticipated, because a larger power law index means that a plate has a smaller ceramic component and that its stiffness is thus reduced. Similar trends are also observed for the CCCC boundary conditions, as shown in Table 12. Figure 17 shows variation of frequency parameter (Ω) versus the power

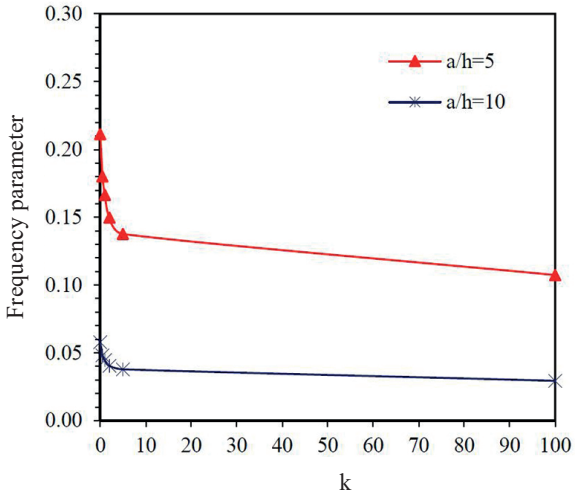

Fig. 17. Variation of Ω vs power law index for different thickness ratios

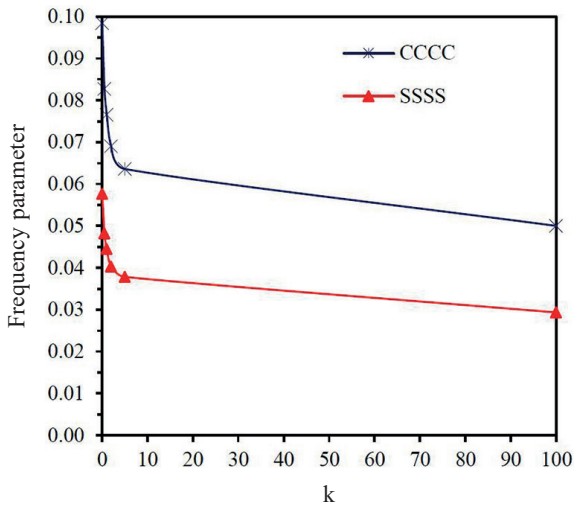

Fig. 18. Variation of Ω vs power law index for different boundary conditions

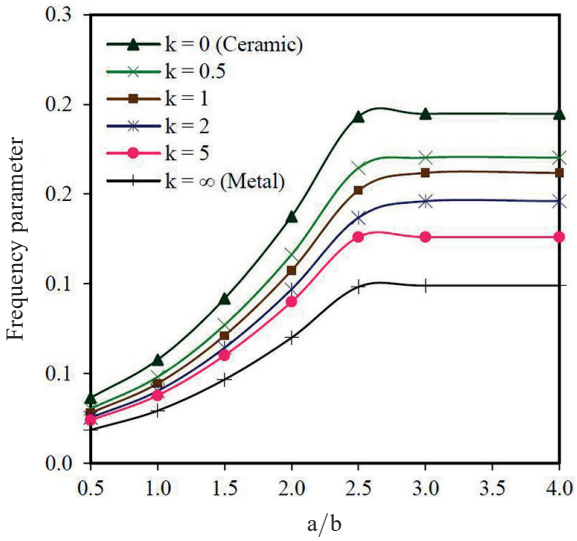

Fig. 19. Variation of Ω vs aspect ratio for SSSS FGM plate

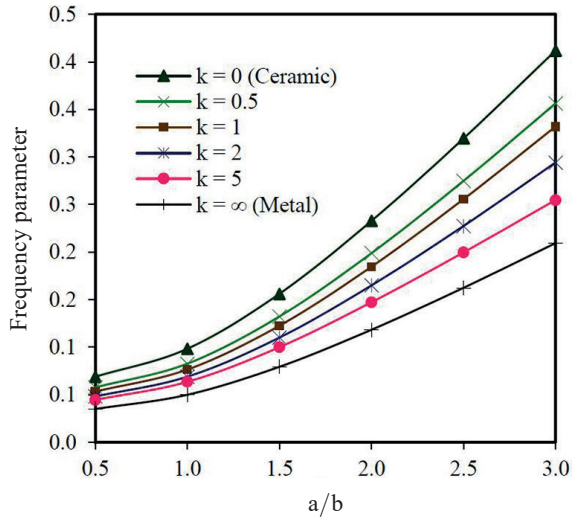

Fig. 20. Variation of Ω vs aspect ratio for CCCC FGM plate

law index for various thickness ratios while Fig. 18 presents the same for the SSSS and CCCC plate.

Since the stability of the CCCC condition is more than SSSS, the frequency parameter is high under the CCCC condition. Figure 19 and 20 indicate the variation of the dimensionless frequency parameter (Ω) versus the aspect ratio for the SSSS and CCCC FGM square plate. It is noted that for the SSSS condition the frequency parameter is not changed beyond the aspect ratio of 2.5 although it keeps increasing with the aspect ratio.

4.5. Analysis of FGM plate under thermal field. The current FE analysis has been attempted to find central deflection of the FGM plate under thermal field for different thickness ratios (a/h = 5, 20, 100) using ANSYS®15.0, hence FGM was used in high temperature environments. In this section, the FGM plate is composed with aluminum as the metal and zirconia as the ceramic component, and individual material properties are presented in Table 2. The results have been obtained for varying temperatures at the top, from 20°C to 300°C, while temperature at the bottom remained constant at 20°C. The results are tabulated in Table 13. They have been validated against Taj et al. [26] when the top surface is at 300°C and the bottom surface temperature is 20°C for different thickness ratios, and the results match considerably, as shown in Table 13. The results also revealed that negative deflection (deflecting in downward direction) of the plate is observed under the thermal field because of the high thermal coefficient with increasing temperature at the top, which is quite opposite in the case of a plate under mechanical loading.

Table 13
Nondimensional central deflection of simply supported FGM plate with different power law index under different top surface temperatures

a/h	Method	Temp. at top	Ceramic	K = 1.0	K = 2.0	Metal
5	Present	20°C	0	-7.25×10^{-4}	-8.20×10^{-4}	0
	Present	50°C	-7.70×10^{-4}	-2.18×10^{-3}	-2.32×10^{-3}	-1.77×10^{-3}
	Present	100°C	-1.92×10^{-3}	-4.82×10^{-3}	-5.14×10^{-3}	-4.40×10^{-3}
	Present	200°C	-4.31×10^{-3}	-1.01×10^{-2}	-1.08×10^{-2}	-9.90×10^{-3}
	Present	300°C	-6.70×10^{-3}	-1.54×10^{-2}	-1.64×10^{-2}	-1.54×10^{-2}
	Taj et al. [26]	300°C	-6.70×10^{-3}	-1.57×10^{-2}	-1.64×10^{-2}	-1.54×10^{-2}
20	Present	20°C	−0	-9.54×10^{-3}	-9.98×10^{-3}	0
	Present	50°C	-1.15×10^{-2}	-3.48×10^{-2}	-3.71×10^{-2}	-2.64×10^{-2}
	Present	100°C	-3.06×10^{-2}	-7.70×10^{-2}	-8.22×10^{-2}	-7.03×10^{-2}
	Present	200°C	-6.88×10^{-2}	-1.61×10^{-1}	-1.72×10^{-1}	-1.58×10^{-1}
	Present	300°C	-1.07×10^{-1}	-2.46×10^{-1}	-2.63×10^{-1}	-2.46×10^{-1}
	Taj et al. [26]	300°C	-1.07×10^{-1}	-2.59×10^{-1}	-2.64×10^{-1}	-2.46×10^{-1}
100	Present	20°C	0	−0.239	−0.250	0
	Present	50°C	−0.286	−0.871	−0.926	−0.658
	Present	100°C	−0.763	−1.923	−2.052	−1.756
	Present	200°C	−1.718	−4.030	−4.310	−3.952
	Present	300°C	−2.673	−6.139	−6.566	−6.148
	Taj et al. [26]	300°C	−2.670	−6.253	−6.586	−6.140

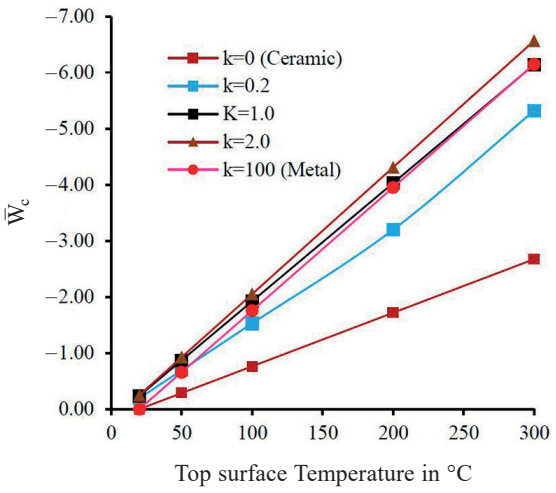

Fig. 21. Variation of nondimensional deflection $\left(\bar{W}_c = W_c/h\right)$ of simply supported FGM thin plate $(a/h = 100)$ by varying top surface temperature and power law index

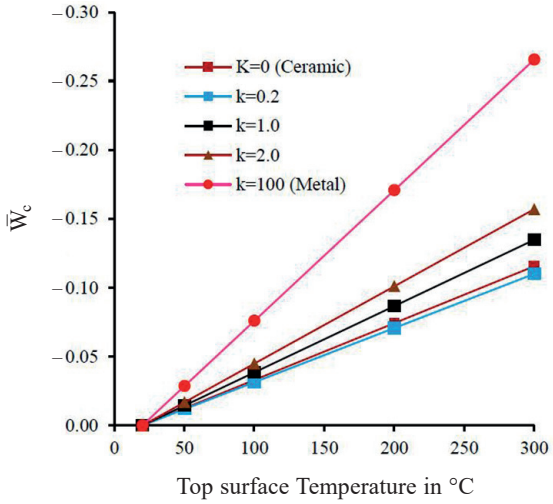

Fig. 22. Variation of nondimensional deflection $\left(\bar{W}_c = W_c/h\right)$ of CCCC FGM thin plate $(a/h = 100)$ by varying top surface temperature and power law index

Figure 21 shows the nondimensional central deflection of the simply supported FGM thin $(a/h = 100)$ plate under varying thermal field. It can be observed that the central deflection of the FGM plate increases linearly with the rising of thermal load. The ceramic phase shows minimum range of deflection changes and due to combination of metal and ceramic components, central deflection falls above the ceramic range. Similar trends have been observed for a clamped FGM plate, as shown in Fig. 22.

5. FE analysis of FGM plate under thermal and mechanical load

In view to producing new results, based on the current FE model using ANSYS®15.0, the static behavior of the FGM plate (Al/ZrO_2) under thermal and mechanical load has been analyzed and tabulated in Table 14. It shows that central deflection is positive for the isotropic material (k = 0 and 100), with top and bottom temperature the same at 20°C. For the remaining k values and top surface temperatures, it is negative due to more expansion in the lower stiffness value along with uniform load $q_0 = -5000\ N/m^2$. Variation of axial stress $\bar{\sigma}_{xx}$ at the top and bottom surface of the FGM plate (Al/ZrO_2) has been evaluated using the current finite element model and established in Table 15. When the isotropic plate is subjected to the mechanical load and thermal field, both top and bottom surfaces experience compressive stress while the composite plate is subjected to tensile stress at the top surface and compressive stress at the bottom surface due to metal segments.

Table 14
Nondimensional central deflection $\left(\bar{W}_c = W_c/h\right)$ of simply supported FGM thin plate $(a/h = 100)$ with different power law index under thermal field (different top surface temperatures) and mechanical load (q_0)

Temp. at top	Ceramic	k = 1.0	k = 2.0	Metal
20°C	0.147	−0.037	−0.033	0.317
50°C	−0.140	−0.662	−0.696	−0.350
100°C	−0.619	−1.717	−1.826	−1.445
200°C	−1.577	−3.827	−4.086	−3.648
300°C	−2.535	−5.937	−6.346	−5.851

Table 15
Nondimensional axial stress $(\bar{\sigma}_{xx} = \sigma_{xx} \times h^2/q_0 \times a)$ of simply supported FGM thin plate $(a/h = 100)$ with different power law index under thermal field (different top surface temperatures) and mechanical load (q_0)

Temp. at top	Ceramic		k = 1.0		Metal	
	Top	Bottom	Top	Bottom	Top	Bottom
20°C	−0.0147	−0.5900	0.0312	−0.5380	−0.0348	−0.6100
50°C	−0.0147	−1.0420	0.3020	−10.2200	−0.0346	−1.0920
100°C	−0.0147	−1.7980	0.7540	−18.5200	−0.0346	−1.8980
200°C	−0.0146	−3.3000	1.6600	−3.5200	−0.0346	−3.5000
300°C	−0.0146	−4.8200	2.5600	−5.2200	−0.0346	−5.1200

6. Conclusions

In this study, the static and dynamic behavior of an FGM plate were examined by means of using the FEA software package, ANSYS®15.0. The following results were obtained from the current finite element studies:

- The validation study reveals the efficiency and capability of the current FE model for analysis of bending, buckling and free vibration behavior of FGM plates with varying power law index, boundary conditions, aspect ratio, thickness ratio and also temperature.

- Displacement decreases with the power law index since stiffness of constituents is decreasing.
- The distributions of shear stresses τ_{xz} through the thickness are not parabolic for the FGM plate when the k value is other than 0 and ∞. This is due to the gradient of materials from ceramic to metal ones.
- The ceramic-rich FGM plate exhibits higher critical buckling load. The critical buckling load is at its minimum in the case of a simply supported plate whereas it is at its maximum in a clamp-supported plate.
- The ceramic-rich FGM plate displays a higher natural frequency parameter than the metal-rich one when the higher thickness ratio (thin plate) shows a lower natural frequency parameter.
- The dimensionless frequency parameter is not changed beyond the aspect ratio of 2.5 for the simply supported plate while it keeps increasing further with the increasing aspect ratio for the clamped support.
- It is also to be noted that negative deflection of the plate is observed under the thermal field, as high thermal expansion with increasing temperature at the top causes the plate to deflect in downward direction.
- When an FGM plate is subjected to both thermal and mechanical load, stresses are changing from compressive to tensile stress at the top surface of the composite plate and deflection is changing from zero to a positive value at the top surface at 20°C.
- The above-obtained results on the static and dynamic behavior of FGM plates observed with varying parameters such as the power law index, thickness ratio, aspect ratio, temperature and types of loads applied are believed to prove useful for designers and researchers who are involved in this particular field.

References

[1] J.N. Reddy, "Analysis of functionally graded plates", *International Journal for Numerical Methods in Engineering,* 47, 663–684 (2000).

[2] L.F.Qian, R.C.Batra, and L.M.Chen, "Static and dynamic deformations of thick functionally graded elastic plates by using higher-order shear and normal deformable plate theory and meshless local Petrov–Galerkin method", *Composites Part B: Engineering* 35, (6–8), 685–697 (2004).

[3] A.M. Zenkour, "Generalized shear deformation theory for bending analysis of functionally graded plates", *Applied Mathematical Modelling* 30, 67-84 (2004).

[4] V. Birman and L.W. Byrd, "Modeling and Analysis of Functionally Graded Materials and Structures" *Applied Mechanics Reviews,* 60, 195-21 (2007).

[5] H. Matsunaga, "Stress analysis of functionally graded plates subjected to thermal and mechanical loadings" *Composite Structures*, 87, 344–357 (2009).

[6] M. Talha and B.N. Singh, "Static response and free vibration analysis of FGM plates using higher order shear deformation theory", *Applied Mathematical Modelling*, 34, 3991–4011 (2010).

[7] M.K. Singha, T. Prakash, and M. Ganapathi, "Finite element analysis of functionally graded plates under transverse load" *Finite Elements in Analysis and Design*, 47, 453–460 (2011).

[8] D.K. Rao, P.J. Blessington, and R. Tarapada, "Finite Element Modeling and Analysis of Functionally Graded (FG) Composite Shell Structures" *Procedia Engineering*, 38, 3192–3199 (2012).

[9] H.-T. Thai and D.-H. Choi, "Finite element formulation of various four unknown shear deformation theories for functionally graded plates" Finite Elements in Analysis and Design, 75, 50–61 (2013).

[10] T.H. Daouadji, A. Tounsi, and E.A.A. Bedia, "Analytical solution for bending analysis of functionally graded plates" *Scientia Iranica B*, 20(3), 516–523 (2013).

[11] J. Yang and Y. Chen, "Free vibration and buckling analyses of functionally graded beams with edge cracks" *Composite Structures*, 83, 48–60 (2008).

[12] X. Zhao, Y.Y. Lee, and K.M. Liew, "Mechanical and thermal buckling analysis of functionally graded plates" *Composite Structures*, 90, 161–171 (2009).

[13] M. Latifi, F. Farhatnia, and M. Kadkhodaei, "Buckling analysis of rectangular functionally graded plates under various edge conditions using Fourier series expansion" *European Journal of Mechanics A/Solids* 41*,* 16-27 (2013).

[14] A. Amiri Rad and D. Panahandeh-Shahraki, "Buckling of cracked functionally graded plates under tension" *Thin-Walled Structures*, 8426–33 (2014).

[15] S. Abrate, "Free vibration, buckling, and static deflections of functionally graded plates" *Composites Science and Technology*, 66, 2383–2394 (2006).

[16] H. Matsunaga, "Free vibration and stability of functionally graded plates according to a 2-D higher-order deformation theory" *Composite Structures*, 82, 499–512 (2008).

[17] X. Zhao, Y.Y. Lee, and K.M. Liew, "Free vibration analysis of functionally graded plates using the element-free kp-Ritz method" *Journal of Sound and Vibration*, 319, 918–939 (2009).

[18] E. Efraim, "Accurate formula for determination of natural frequencies of FGM plates basing on frequencies of isotropic plates" *Procedia Engineering*, 10, 242–247 (2011).

[19] R. Javaheri and M.R. Eslami, "Buckling of functionally graded plates under in plane compressive loading". *ZAMM Journal*, 82(4), 277–283 (2002).

[20] F. Chu, J. He, L. Wang, and Z. Zhong, "Buckling analysis of functionally graded thin plate with in-plane material inhomogeneity" *Engineering Analysis with Boundary Elements*, 65, 112–125 (2016).

[21] P. Malik and R. Kadoli, "Thermo-elastic response of SUS316-Al_2O_3 functionally graded beams under various heat loads", *International Journal of Mechanical Sciences*, 128-129, 206-223 (2017).

[22] M. Chmielewski and K. Pietrzak, "Metal-ceramic functionally graded materials– manufacturing, characterization, application, *Bull. Pol. Ac. Tech.*, 64(1), 151–160 (2016).

[23] K.K. Zur, "Green's function approach to frequency analysis of thin circular plates", *Bull. Pol. Ac. Tech.*, 64 (1), 181–188 (2016).

[24] S.P. Timoshenko and S.W. Krieger, "Theory of Plates and Shells", second edition, *McGraw-Hill International Editions*, (1959).

[25] D.-G. Zhang and Y.-H. Zhou, "A theoretical analysis of FGM thin plates based on physical neutral surface", *Computational Materials Science*, 44, 716–720 (2008).

[26] M.N.A. Gulshan Taj, A. Chakrabarti, and A.H. Sheikh, "Analysis of functionally graded plates using higher order shear deformation theory", *Applied Mathematical Modelling,* 37, 8484-8494 (2013).
[27] D.-G. Zhang, "Modeling and analysis of FGM rectangular plates based on physical neutral surface and high order shear deformation theory", *International Journal of Mechanical Sciences*, 68, 92–104 (2013).
[28] R. Lal and N. Ahlawat, "Axisymmetric vibrations and buckling analysis of functionally graded circular plates via differential transform method" *European Journal of Mechanics / ASolids*, 52, 85–94 (2015).
[29] H. Parandvar and M. Farid, " Large amplitude vibration of FGM plates in thermal environment subjected to simultaneously static pressure and harmonic force using multimodal FEM", *Composite Structures*, 141, 163–171 (2016).
[30] K.K. Zur, "Quasi-Green's function approach to free vibration analysis of elastically supported functionally graded circular plates", *Composite Structures*, 183, 600–610 (2018).
[31] K.K. Zur, "Free vibration analysis of elastically supported functionally graded annular plates via quasi-Green's function method", *Composites Part B*, 144, 37–55, (2018).